Simulation of Multi-Axis Machining Processes Using Z-mapping Technique

O. M. Ozkirimli, L. T. Tunc, E. Budak
Manufacturing Research Laboratory (MRL), Sabanci University, 34956, İstanbul, Turkey

Abstract
Parameter selection in machining operations is curial for product quality and high productivity. Process parameters such as feed, spindle speed and depth of cuts are often chosen by trial-error methods. Mathematical models can be employed to predict the mechanics and the dynamics of the process. In this study, Z-mapping technique is utilized to simulate the process step by step by updating the workpiece according the given tool path where the cutter engagement areas are also determined. Using the numerical generalized process model, whole process is simulated for any milling tool geometry including intricate profiling tools, serrated cutters and tools with variable edge geometries.

Keywords: Modeling, Milling, Simulation, Cutting forces, 5-axis milling

1 INTRODUCTION

The objective of all machining operations is to be as productive as possible by satisfying desired tolerances and surface quality. In general, the process parameters controlling the rate of production are chosen using trial and error based methods which mainly depend on the experience. However, poor choices of machining parameters may result in low productivity or stall of the machine tools, excessive part and tool deflections or tool breakages due to high cutting forces. In order to determine optimal cutting parameters, process models and simulations can be employed to predict key aspects of machining operations such as cutting forces and vibrations.

In milling operations, there are many alternative methods to machine a part considering the choice of milling tool, process parameters and machining strategies. Finding an optimal solution might not be possible; however, through process modeling feasible sets of solutions can be simulated and chosen.

The kinematics of milling process was first analyzed in detail by Martelotti [1]. Koenigsberger and Sabberwal [2] developed equations for milling forces using mechanistic modeling which was followed by Kline et. al. [3] Later, Altintas and Spence [4] developed a semi-analytical force model which can be integrated into CAD systems. Budak et al. [5] proposed an approach where cutting coefficients obtained from orthogonal database are transformed into helical milling considering the oblique cutting mechanics. Employing this model, Lee and Altintas modeled the mechanics and dynamics of helical flat end cutters [6] and later improved their model to calculate cutting forces for ball end mill tools [7]. For standard milling tools, the first complete geometrical model was developed by Engin and Altintas [8] covering all standard end mill geometries. They modeled helical cutting edge geometries wrapped around these tools and analyzed the mechanics and dynamics of cutting by verifying their model experimentally.

Serrated milling tools are used extensively for roughing operations due to their high material removal rate performance. The advantage of the serrated cutters is that their wavy cutting edge profile and axial phase shift of the wave between consecutive teeth induces irregular chip removal rate. This irregularity increases chip breakage and cutting stability drastically. Tlusty et al. [9] were the first researchers investigating the chatter stability of the serrated milling cutters where they examined non-helical (straight) fluted cutter geometries. Campomanes [10] established a mechanic and dynamic model for helical serrated cutters with sinusoidal wave form. He formulated the uncut chip thickness for serrated cutters and proposed a dynamical model based on [11] where the effect of serration form was taken as an average regeneration quantity. Merdol and Altintas [12] developed a model for serrated flat, ball and taper end mils utilizing B-spline representation for the serration waves. Zhang et. al. [13] developed a sectional numerical model to identify cutting forces and effective cutting force coefficients.

For multi-axis machining, due to the variation in tool position and orientation, the models have to consider in-process workpiece geometry. One of the most challenging parts in multi-axis milling process modeling is to predict the cutter engagement boundaries during cutting. Both analytical and numerical methods are present in the literature; however analytical models are very limited due to complexity of the multi-axis machining operations. For 3 axis milling of sculptured surfaces, Lazoglu and Liang [13] presented an analytical approach to predict the engagement boundaries. This model was verified by airfoil machining experiments. Z-mapping and Octree methods are among the most popular and robust numerical models proposed in the literature. In Z-mapping method [14]-[15] the workpiece is represented with arbitrary vectors in the Z direction and the height of these vectors is updated by the intersection of the swept volume of the cutter body during cutting. In Octree method, the workpiece is divided into cubic elements and as in the Z-mapping methodology arbitrary cubes engaging with the swept volume of the cutter are further decreased in size to finally find an accurate solution. There are also a few analytical models developed for mostly case specific or tool specific conditions. For 5-axis milling, an analytical engagement model considering the orientation of the cutting tool was developed by Ozturk and Budak [17]. They also predicted the cutting forces and form errors during multi-axis operations. Another case specific semi-analytical model for taper ball end

mills was developed by Ferry and Altintas [19]. All of these models for multi-axis machining are limited to specific cases for designated milling conditions.

In this paper, a very general multi-axis process model which can handle any tool geometry and surface form is proposed. In the next section, the determination of the tool and workpiece using the Z-mapping technique is given. The process model and the test results are presented in section 3 which is followed by experimental verification results in section 4.

2 TOOL-WORK ENGAGEMENT BY Z-MAPPING

In this study, the approach of Z-mapping method is adopted for determination of engagement boundaries and updating of the in-process workpiece geometry. The important steps of application of the Z-mapping method for determination of tool-workpiece engagement boundaries are summarized in Figure 1. The rough workpiece information is obtained in STL format, whereas the cutting tool information is obtained using the general tool geometry information as described in section 3.1. Then, the workpiece geometry is converted into bunch of vectors on an equally spaced grid, storing the Z values of the workpiece geometry. The mapping is done using the STL information of the faces covering the rough workpiece geometry. The information of each face is generated on separate STL files and used in the calculations. The solid model of the cutting tool is divided into number of patches each consisting of four points on the tool envelope. Finally, the workpiece is updated by finding the vectors cut by the tool swept volume at each position of the cutter. In order to find the height of a Z nail the intersection on the –xy grid and the triangular facets are calculated. At this point, it is noteworthy to state that in general, each nail intersects each facet unless they are parallel. Thus, the height of each nail is the minimum of the distances to every facet.

2.1 Modeling of tool geometry and tool motion

The position and orientation of the cutting tool is parsed from the CL file, where the x, y, and z coordinates of the tool tip and i, j, k components of the unit tool axis vector are provided as shown in Figure . The points on the cutter envelope are calculated according to the general tool geometry as described in section 3. However, it is required to translate and orient the points according to the tool position and tool axis at each tool move. This is done in the following manner; first the cutter is modeled, i.e. the points on the envelope are calculated at and initial position (0, 0, 0), where the center of the spherical part of the tool is the origin and initial tool axis vector is [0, 0, 1]. Then, the rotations of the initial tool axis vector around i and j vectors, i.e. [1, 0, 0] and [0, 1, 0] are determined analytically using an inverse solution of the rotation operation at each tool position. Finally, the points are rotated around the tool center and translated to the coordinates provided by the CL file. An illustration of this approach is given in Figure 3. The unit tool axis vector can be considered to be formed by concatenation of two fixed axis rotations of the initial orientation vector [0,0,1] around j and i axis, respectively. Rotation of a vector about any unit vector is performed using the following transformation matrix;

$$R(\vec{\mathbf{u}},\theta_u)=\begin{bmatrix} u_i^2+\left(1-u_i^2\right)C & u_iu_jV+u_kS & u_iu_kV-u_yS \\ u_iu_jV-u_kS & u_j^2+\left(1-u_j^2\right)C & u_ju_kV+u_iS \\ u_iu_kV+u_jS & u_ju_kV-u_iS & u_k^2+\left(1-u_k^2\right)C \end{bmatrix} \quad (1)$$

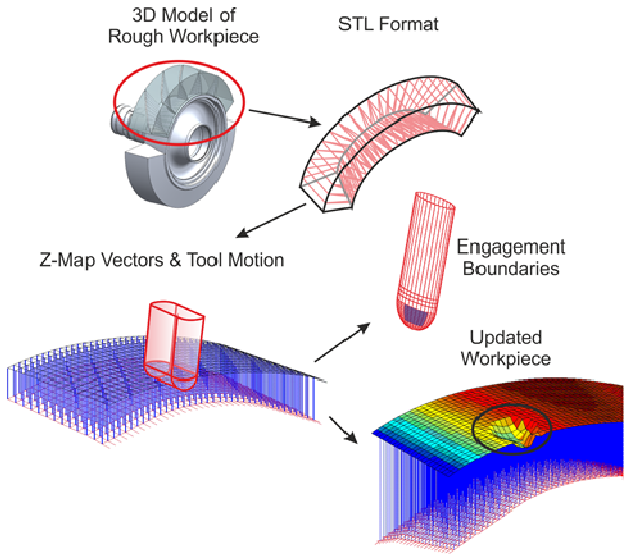

Figure 1: Application of Z-map method.

x	y	z	i	j	k
GOTO/-72.5462,254.0000,63.0866,-0.4882140,0.8029930,0.3418330					
GOTO/-16.8187,162.3419,24.0679,-0.4882140,0.8029930,0.3418330					
GOTO/-15.5786,160.3023,23.1996,-0.4882140,0.8029930,0.3418330					
GOTO/-13.5483,160.2419,21.9026,-0.4882140,0.8029930,0.3418330					
GOTO/-13.1423,160.2298,21.6433,-0.4882140,0.8029930,0.3418330					
GOTO/-11.1120,160.1694,20.3462,-0.4882140,0.8029930,0.3418330					

Figure 2: A sample CL file

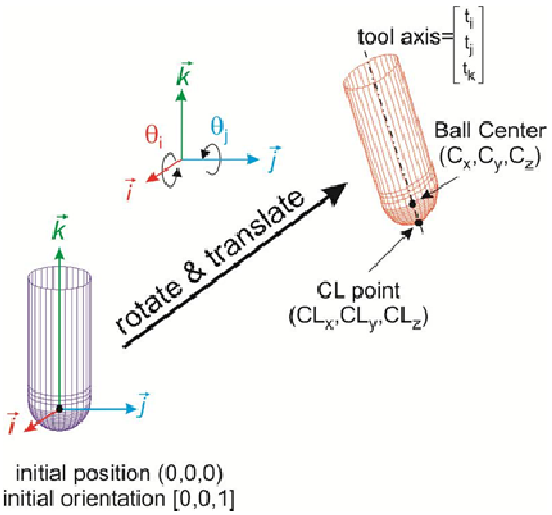

Figure 3: Modeling of tool motion.

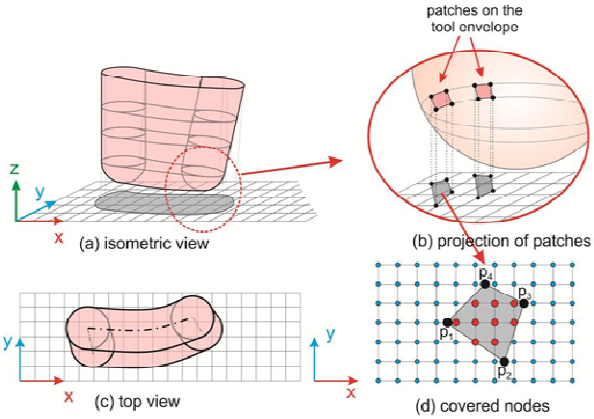

Figure 4: The projection of tool swept volume on –xy grid.

In Figure 4, the red points represent the locations of the nails covered by the projected polygon area. Identifying the points enclosed by the polygon formed by points p1, p2, p3 and p4 (see Figure 4.d) becomes a problem of determining whether a series of points lie within the bounds of a polygon in 2D plane. A simple implementation of this method requires each wall intersection be checked for each point, resulting in an O(N*M) operation count, where M is the number of edges of the polygon and N is the number of points to be tested. There are two advantages of the implemented algorithm. First, the test points are sorted by the y-value and a binary search is used to find the first point in the list that has a chance of intersecting with a given wall. The sorted list is also used to determine when we have reached the last point in the list that has a chance of intersection. This means that in general only a small portion of points are checked for each wall, rather than the whole set. Secondly, the intersection test is simplified by first checking against the bounding box for a given wall segment. Checking against the bounding box is an inexpensive alternative to the full intersection test and allows us to take a number of shortcuts, minimizing the number of times the full test needs to be done.

The engagement boundaries, i.e. the patches of the cutting tool engaged with the workpiece, are then provided to the force model where they are converted to engagement maps in immersion angle domain for simulation of cutting forces.

3 CUTTING FORCE MODEL

In this study, milling tools are geometrically defined as a point cloud representing the outer envelope of the tool and the cutting edges. Through calculating the instantaneous cutting forces acting on each tooth point, the total forces are calculated using the linear edge force model.

3.1 Cutting Tool Geometry

The cutting tool is presented in tool coordinate system, *xyz* where *x*, *y* and *z* defines the feed, cross-feed and tool axis directions, respectively. The cutter is divided into axial elements along the tool axis direction and the points on the axial sections are represented in polar coordinates as shown in Figure 5. A point *P* on a helical cutting flute is defined in cylindrical coordinates by characterizing radial distance *r(z)*, the axial immersion angle *κ(z)* which is the angle between the tool axis and the normal vector of the cutting edge and the radial lag angle *ψ(z)*.

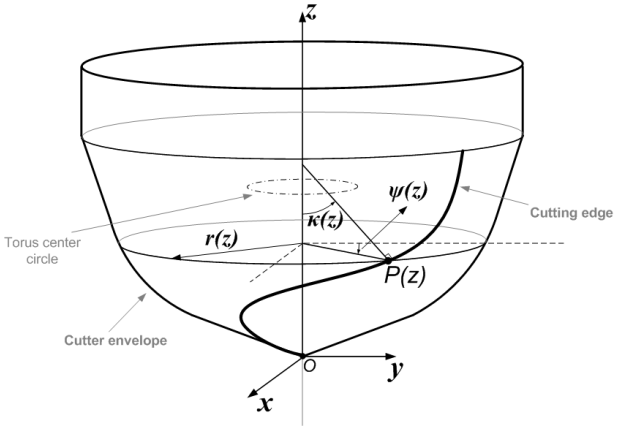

Figure 5: Milling tool and corresponding geometrical parameters

Due to helical cutting flutes, cutting points at different elevations are shifted rotationally along the periphery of the cutter body with respect to each other. This rotational shift at elevation *z* is defined as the lag angle, *ψ(z)*. The relation between the lag angle and rotation angle ϕ of the tool during cutting defines the exact definition of the immersion angle of the corresponding cutting tooth.

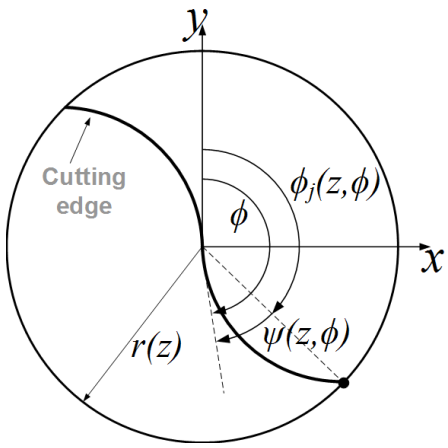

Figure 6: Lag angle and immersion angle definition for a cutting flute

For general cutting tools with variable helix and variable tooth pitch separation, generalized local immersion angle $\phi_j(z)$ definition of the j^{th} cutting edge is then given as;

$$\phi_j(z) = \phi + \phi_{p,j} - \psi_j(z) \quad (2)$$

where $\phi_{p,j}$ and ψ_j represent the angular position of j^{th} cutting edge with respect to the previous $j\text{-}1^{th}$ edge (pitch angle) and the axial lag angle shift of the j^{th} cutting edge having a specific helix angle, respectively.

A milling tool can be considered as a union of basic geometric 3D units which are tori and cones. Each basic unit defines a segment of the milling tool. These basic geometric units can be constructed as a revolve surface where the required contour defines the outer body of the milling tool. Most standard milling tools can be expressed as a union of three or less segments, and can therefore be represented parametrically. However, parametric representation of custom tools with intricate multi segmented (union of more than three basic geometric unit) geometries is not an efficient way to define the tool geometry because of the large amount of parameters required for each segment. It is convenient to obtain the geometric properties of the cutter envelope by decoding the CAD data. Once the segment envelope information is known, the points on the cutter envelope can be calculated parametrically along the tools axis at each dz elevation step and revolving the calculating point around the tool axis with dϕ angular increment gives the 3D point cloud of the cutter. The cutter envelope is modeled in a CAD environment as a combination of lines and arcs corresponding to each segment. IGES data format is adequate for obtaining the boundary information of the individual segments. In Figure 7, an exemplary multi-segmented tool geometry involving 4 arcs and 5 lines with corresponding geometrical parameters is given. Lines are represented with S_i and E_i points being start and end points, respectively. In addition to S_i and E_i, arcs are represented with an additional center point C_i where index *i* denotes the segment number starting from the tool tip.

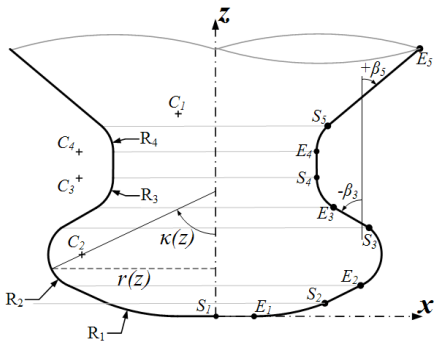

Figure 7: Multi-segmented tool geometry with corresponding segment parameters

Considering a linear segment profile, the radial distance *r(z)*, the axial immersion angle *κ(z)* are given as;

$$\left.\begin{aligned} r(z) &= \frac{z - S_{i,z}}{\tan \beta_i} + S_{i,x} \\ \kappa(z) &= \beta_i \end{aligned}\right\} \tag{3}$$

where β_i is the inclination angle of the line segment.

For a tapered conic part represented with a line segment, the lag angle definition is given as;

$$\psi_L = \frac{\ln\left(r(z)\right)\tan i_0}{\sin \beta_i} \tag{4}$$

A circle segment represents a torus unit element in the cutter body. For a torus, the radial distance *r(z)*, the axial immersion angle *κ(z)* are given as follows;

$$\left.\begin{aligned} r\left(z\right) &= \sqrt{R^2 - \left(R_{z,s} - z\right)^2} \\ \kappa\left(z\right) &= \sin^{-1}\left(\frac{r\left(z\right) - R_{r,s}}{R}\right) \end{aligned}\right\} \tag{5}$$

and the lag angle expression for the arc segment is;

$$\psi_A = \frac{(R_i - C_{i,z} + z)\tan i_0}{R_i} \tag{6}$$

Final lag angle at elevation *z* is calculated with respect to current and previous segment definitions to ensure continuity;

$$\psi(z) = \psi_{L/A} + \psi_{pre} - \psi_{cur} \tag{7}$$

where ψ_{pre} is the final lag angle of the previous segment at the starting point of the current one and ψ_{cur} is the lag angle of the current segment at its starting point.

Although, the profile geometry constitutes the major part of the operation, hence the process simulation, the helical flute geometry and its variations play a bigger role in the mechanics and dynamics of the process. The time delay differences between adjacent cutting flutes removing material affects the cutting forces but more importantly disturbs the regenerative chatter mechanisms. In this section, the geometrical variation and non-uniform distribution of helical flute geometries will be given and a general formulation encompassing all possible variations will be introduced.

Variation of helix angle from flute to flute and the pitch angle between adjacent teeth changes the immersion angle definition which directly effects the time delay at each elevation level and as a consequence the chip thickness variation. Equation 2 can be examined in two parts in this scope. First, the variation of the pitch angle $\phi_{p,j}$ and secondly, the lag angle $\psi_j(z)$ depending on helix angle of the j[th] cutting edge, $i_{o,j}$. In Figure 8, a 4 fluted flat end mill with variable helix and variable pitch angles is shown to identify previously mentioned parameters.

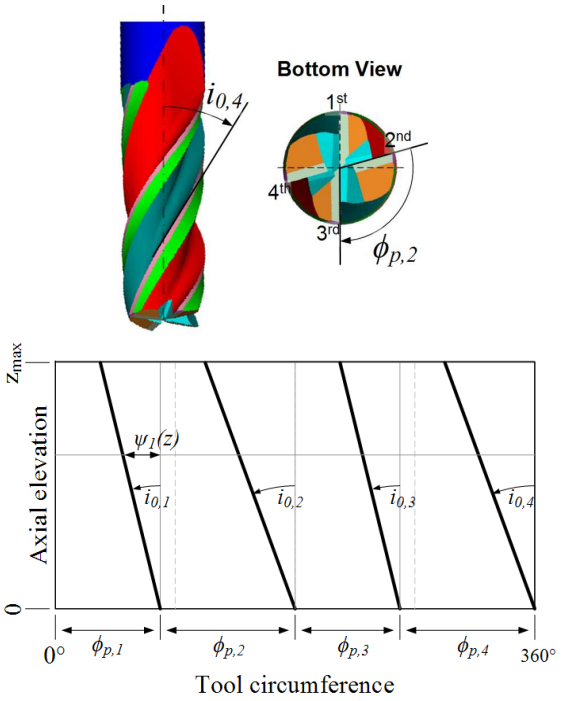

Figure 8: Cutting flute geometry and corresponding parameters; (a) 3D representation, (b) Unfolded representation

In order to find the delay between each flute at elevation *z*, the separation angle, $\delta\phi_j(z)$ is calculated for each axial level, *z*. The separation angle defines the flute geometry of the cutting tool from tool axis to the cutting edge for flute *j*. It is calculated as the difference of immersion angles for the *j[th]* and the *j+1[th]* cutting flutes;

$$\delta\phi_j(z) = \phi_{j+1}(z) - \phi_j(z) \tag{8}$$

3.2 Uncut chip thickness formulation for general milling tools variable flute geometry

Chip thickness in milling operations is defined as the length of the material removed during trochoidal rotary movement by a cutting flute from the previously machined surface in tool surface normal direction. The trochoidal motion can simply be assumed as a positional shift along the feed vector having a magnitude of effective feed per tooth length $f_{t,j}$. This approximation is valid for large tool diameter over feed per tooth ratios which is generally the case for non-micro tools. Mathematically, for general milling tools performing multi-axis milling operations the chip thickness $h_j(\phi_j,z)$ is defined as:

$$h_j(\phi_j, z) = (\hat{n} \cdot \hat{f})\, f_{t,j} \tag{9}$$

where $\hat{f}$ is the feed unit vector in tool coordinates *xyz*. As a convention the feed vector is always considered in plane with tool *x* direction. Thus, the feed unit vector in

tool coordinates can be represented in a vector form as a combination of planar feed $\hat{f}_x$ and axial feed $\hat{f}_z$;

$$\hat{f} = \begin{bmatrix} \hat{f}_x \\ 0 \\ \hat{f}_z \end{bmatrix} \tag{10}$$

The cutting edge point unit outward vector $\hat{n}$ is defined as

$$\hat{n} = \begin{bmatrix} \sin\kappa \sin\phi_j \\ \sin\kappa \cos\phi_j \\ -\cos\kappa \end{bmatrix} \tag{11}$$

where κ or in long form $\kappa_j(z)$ and ϕ_j or in long form $\phi_j(\phi,z)$ are the axial and radial immersion angles.

Evaluating the general chip thickness equation 9, two separate parts are generated: chip thickness in planar direction and in axial direction;

$$h_j(\phi_j, z) = (\hat{f}_x \sin\phi_j \sin\kappa - \hat{f}_z \cos\kappa) f_{t,j}(z) \tag{12}$$

For milling tools having N_t number of cutting edges with constant distribution (non-variable helix and pitch angles), the feed per tooth value is simply expressed as;

$$f_{t,j}(z) = \frac{feed}{n.N_t} \tag{13}$$

where *feed* is the feed rate in mm/min and *n* is the spindle speed value in rpm. This results in even distribution of material to be removed in one revolution by all cutting edges. Variable helix and pitch angles introduce varying delay between successive cutting edges resulting in varying chip thickness. The originating feed per tooth value can thus be expressed as follows

$$f_{t,j}(z) = \frac{feed}{n} \frac{\delta\phi(z)}{2\pi} \tag{14}$$

In Figures 9 and 10, the comparison between chip load of a non-variable tool and variable helix and pitch angle tool is given. For both cases milling tools with 4 cutting edges are modeled and the process is a half immersion down milling operation with feed over spindle ratio 0.4mm. For the non-variable tool with constant 30° helix angle for all of the cutting edges, the maximum chip load is equal to 0.05mm/tooth (Figure 9). The simulated variable tool in Figure 10 has a helix distribution of 30°-36°-30°-3 6° and the pitch angle variation *ΔP* for alternating pitch is set to 10°. Due to the variation of the cutting edge prope rties the instantaneous chip thickness value differs both from one cutting edge to another as well as along the cutting edge itself.

For serrated cutters, the local radius at each cross-section of the tool for each cutting edge is different from each other due to wave form in the radial direction. Moreover, serrated milling cutters are ground radially with a wave form. Similar to a tapping tool, the radial profile is ground in a helical form causing phase difference in the wave profile with the adjacent cutting flutes. In Figure 11, the phase difference between adjacent teeth is demonstrated. For equally separated milling cutters the phase shift can be denoted as;

$$\theta_{s,j} = 2\pi \frac{j-1}{N_t} \tag{15}$$

where j is the tooth number starting from 1.

For serrated milling tools, both the variation of local radius along the cutting edge and the phase difference of the serration wave form for each cutting edge vary along the tool axis. During cutting, some parts of the cutting edges do not engage with the surface machined by the previous edge.

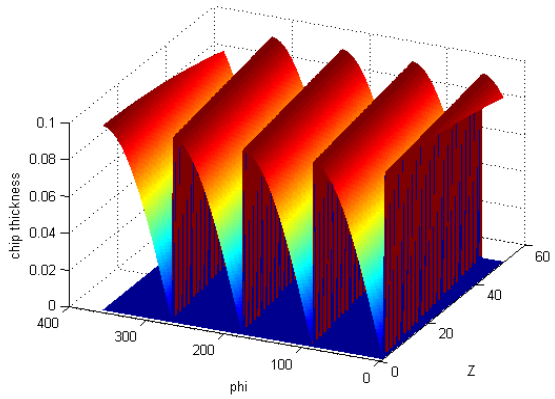

Figure 9: Chip load on a conventional milling tool.

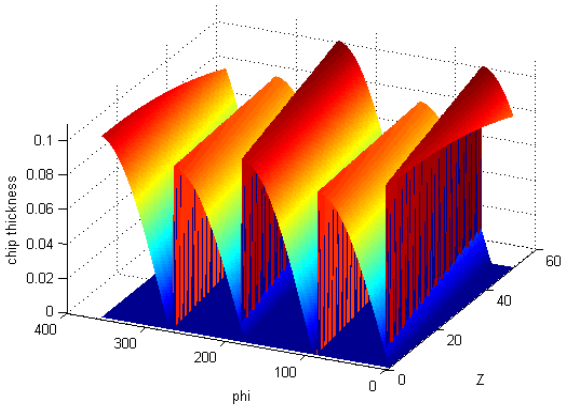

Figure 10: Chip load on a variable helix/pitch milling tool.

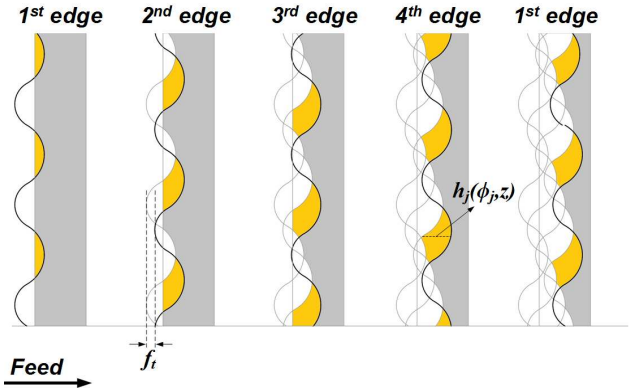

Figure 11: Chip load on a serrated cutter having equally separated circular wave formed edges

The chip thickness variation of a serrated cutter can be investigated as if the cutter has a known run-out function along the tool axis. The definition of the uncut chip thickness for a serrated cutter performing 2½ axis operations is given as follows;

$$h_j(\phi_j, z) = \min_{m=1...N_t} \left[\frac{\left(\sum_{p=1}^{m} f_{t,j}(z) \right) \sin(\phi_j) + ...}{r_j(z) - r_{j-m}(z)} \right] \sin\kappa_j(z) \quad (16)$$

If the feed per tooth value is larger than the difference of the local radii of the cutting edges (in other words; the wave amplitude of the serration profile) the serration profile is not effective anymore because the $r_j(z) - r_{j-m}(z)$ term in the chip thickness definition along the whole axial level becomes less than the effective uncut chip thickness:

$$\left(\sum_{p=1}^{m} f_{t,j}(z) \right) \sin(\phi_j) < r_j(z) - r_{j-m}(z) \quad (17)$$

if the above expression is not satisfied then the whole cutting edges engage with the workpiece. Hence, using serrated cutters the feed per tooth must be chosen according to the wave amplitude of the serration profile. Equation (16) is only valid for tools performing a 2½ axis operation where a point on the cutting edge at elevation *z* is always cutting the previously machined surface generated by a previous edge point at the same elevation level *z*. When the tool performs a multi-axis operation, the exact same cross-section points do not coincide. This issue can be neglected for straight fluted cutters because regarding the angular and axial discretization steps of the simulation, the discrete zone can be assumed as two parallel lines depicting previous and cutter edges even though the tool might be a multi-segmented one. However, for serrated cutters with small wave length, the discretization may not be fine enough to deal with the explained issue. The problem is depicted in Figure 12 where the feed vector direction is shown by *f*, the numbers indicate the numeration of cutting edges and corresponding edge points to consider in order to calculate uncut chip thickness.

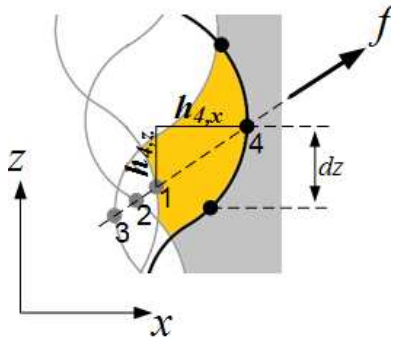

Figure 12: Detailed uncut chip thickness definition for a serration profile

Therefore, the definition for the uncut chip thickness in *x* direction for a serrated general milling cutter should be updated as follows;

$$h_{j,x}(\phi_j, z) = \min_{m=1...N_t} \left[\left(\sum_{p=1}^{m} f_{t,j}(z) \right) \hat{f}_x \sin\phi_j + \Delta r_{eff} \right] \sin\kappa_j(z) \quad (18)$$

where the effective radius difference, Δr_{eff} is defined as;

$$\Delta r_{eff} = r_j(z) - r_{j-m}\left(z - \left(\sum_{p=1}^{m} f_{t,j}(z) \right) \hat{f}_z \right) \quad (19)$$

On the other hand, the uncut chip thickness in *z* direction is not affected by this mechanism:

$$h_{j,z}(\phi_j, z) = \left(\hat{f}_z . f_{t,j}(z) \right) \cos\kappa(z) \quad (20)$$

Finally, the definition of uncut chip thickness for a general serrated variable helix and pitch cutter is given as;

$$h_j(\phi_j, z) = h_{j,x}(\phi_j, z) - h_{j,z}(\phi_j, z)$$

$$h_j(\phi_j, z) = \min_{m=1...N_t} \left[\frac{\left(\sum_{p=1}^{m} f_{t,j}(z) \right) \hat{f}_x \sin\phi_j + ...}{\Delta r_{eff}} \right] \sin\kappa_j(z) \quad (21)$$
$$- \left(\hat{f}_z . f_{t,j}(z) \right) \cos\kappa(z)$$

4 EXPERIMENTAL RESULTS AND MODEL VERIFICATION FOR DIFFERENT MILLING TOOLS

4.1 Ball end mill

First 5-axis milling test case involves cutting Ti_6Al_4V workpiece with a standard ball end mill tool. The tool and process properties are given in Table 1.

Table 1: Tool and process properties for ball end mill verification test

Tool (Ball end mill)

Radius R	***Edge # N_t***	***Helix angle i_0***
6mm	2	30°

Process

Axial DoC	***Radial DoC***	***Lead angle***	***Tilt angle***	***Feed***	***Spindle speed***
1.5mm	slotting	+10°	-15°	600mm/min	3000rpm

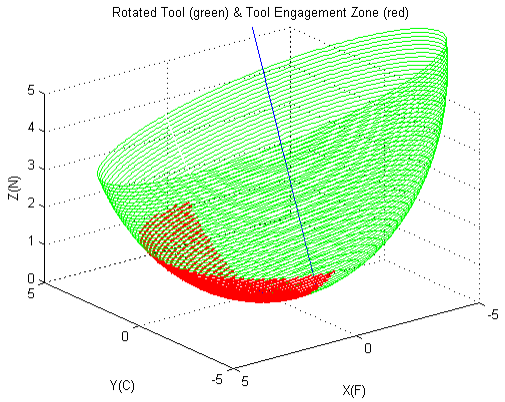

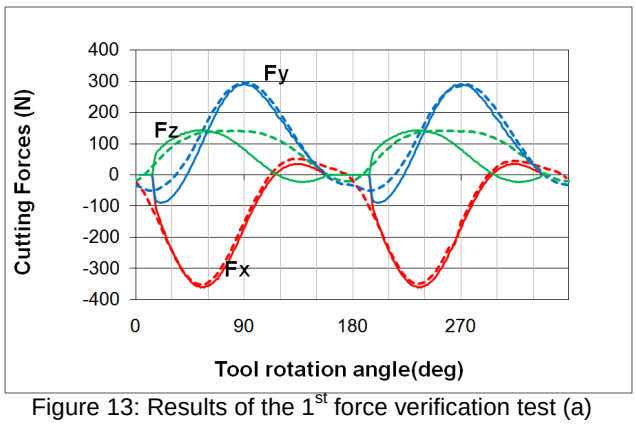

Figure 13: Results of the 1st force verification test (a) cutter engagement zone (b) simulated versus measured forces (simulated in thin line, measured in dashed)

The material database for Ti_6Al_4V generated by Budak et al. [5] was used in the simulations. In Figure 13, the cutter engagement boundaries and the comparison of measured and simulated forces which show good agreement are given.

4.2 Multi segmented tool

In order to verify the presented multi segmented tool definition, a custom profiling tool provided by Makina Takım Endüstrisi (MTE) is utilized. The tool profile geometry is extracted using an optic CMM machine (Dr. Schneider WM1 400) and the representative profile directly taken from the CMM is given in Figure 14.

(a) (b)

Figure14: Custom profiling tool (a) CMM output of the profile for the custom multi-segmented tool, (b) actual tool.

The tool has straight 18 cutting edges and the tool profile is composed of 8 linear and 4 circular segments. Tool diameter and height are measured as 68.3mm and 20.2mm, respectively. These types of custom profiling tools are often utilized for slotting in order to engrave the edge profile directly to the material. For this reason, the verification test should be a 2½ axis operation where the axial depth of cut is chosen greater or equal to the tool length. In the test case, an Al7075-T6 workpiece is cut and tool and process properties are given in Table 2. In Figure 15, the comparison of measured and simulated forces is given together with the corresponding cutter engagement boundaries. In simulations, 0.2mm of axial elevation step size (*dz*) and 1° of rotation angle step size is utilized to capture the geometric variation of the cutting tool segments. Simulation and experimental results are in good agreement where the basic trend and peak force amplitudes are satisfied. On the other hand, there exists a small delay in the tooth periods between the simulated and measured forces which can be due to the deviation in the spindle speed during cutting.

Table 2: Tool and process properties for multi-segmented tool verification test

Tool (Custom profiling tool)

Profile geometry	*Tool diameter*	*Tool height*	*Edge # N_t*	*Helix angle i_o*
Figure	68.3mm	20.2mm	18	0°

Process

Axial DoC	***Type***	***Radial DoC***	***Feed***	***Spindle speed***
20.2mm	down milling	2mm	1260mm/min	1400rpm

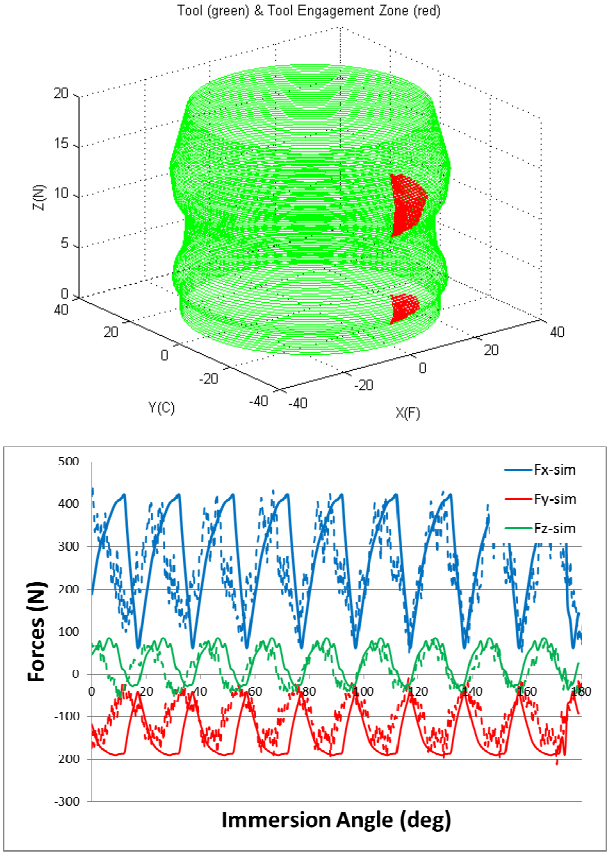

Figure 15: Results of the multi-segmented tool force verification (a) cutter engagement zone (b) simulated versus measured forces (simulated in thin line, measured in dashed)

4.3 Serrated Tool

In the following verification test, the cutting forces measured in milling of AL7075 – T6 using a serrated end mill with circular serration profile are compared to the simulated ones. The cutting tool has a circular serration profile defined by the DIN 844 NF standard. The geometrical tool parameters are given in Table 3. In order to demonstrate the effect of chip thickness several cases with different feed rates were tested. The test conditions for two representative experiments are given in Table 4.

Table 3: Tool properties for serrated flat end mill

Tool diameter	*Edge # N_t*	*Helix angle i_0*	*Serration profile type*
12mm	3	30°	Circular A_0 = 0.3mm ω_s = 2mm

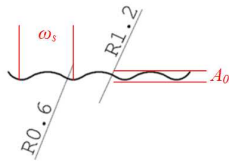

Serration Geometry

Table 4: Process conditions for serrated end mill force verification tests

Axial DoC	*Type*	*Radial DoC*	*Spindle speed*	*Feed rate*
4mm	down milling	9mm	1200rpm	0.015mm/tooth 0.075mm/tooth

In Figure 16, the simulated and measured forces are compared for two different feed values. The results show good agreement.

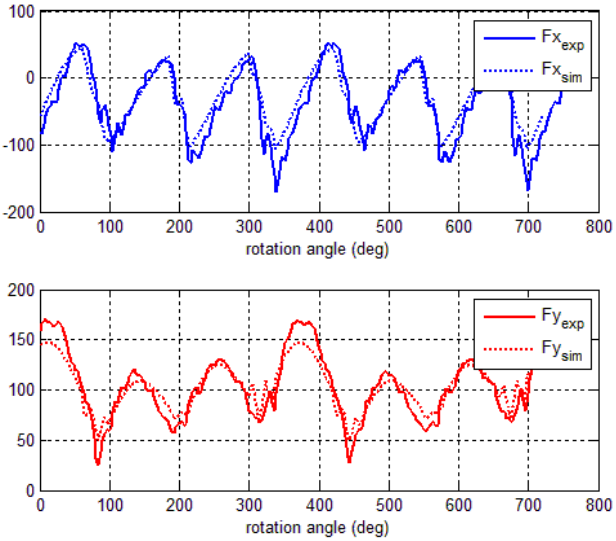

Figure 16: Force verification results for serrated end mills.

4.4 Process simulation of a full cutting cycle employing Z-mapping

In order to verify the process simulation employing Z-mapping, four different cases are considered. A Ti6Al4V block is machined using a carbide ball end mill with a diameter of 12mm, 2 cutting flutes and 30° helix angle. The surface is machined following linear tool paths to achieve a sinusoidal face profile. The cutting parameters are shown in Table 4.

In Figure17, a virtual CAM operation and resulting machined surfaces using NX7.5 is shown. First three operations (I, II, III) involve cutting an intact surface whereas in the IVth operation a previously machined surface is cut diagonally.

Table 4: Cutting conditions for process simulation verification tests

	Step no	*Cutting type*	*Lead*	*Tilt*
I	1	Slotting	0	0
	2	%50 radial	0	0
	3	%50 radial	0	0
II	4	Slotting	15	25
	5	%50 radial	15	25
	6	%50 radial	15	25
III	7	Slotting	15	25
	8	%50 radial	15	25
IV	9	Slotting	20	30
	10	%50 radial	20	30

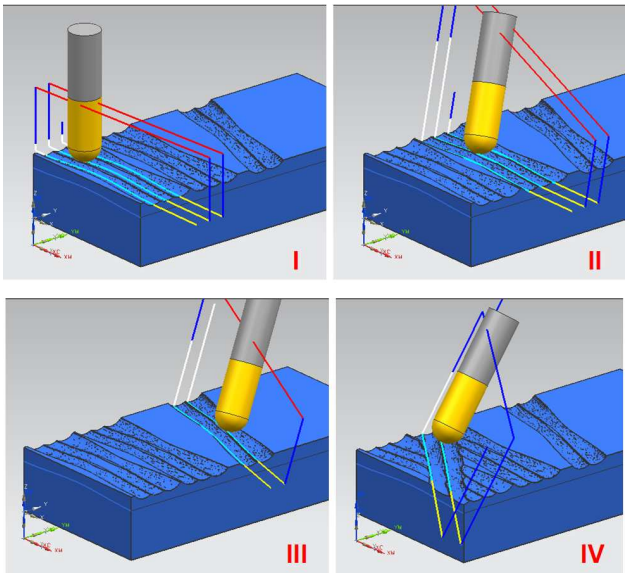

Figure 17: Virtual CAM operation and resulting surfaces

In order to capture details of the process, and to be able to determine engagement boundaries accurately the STL solid body is mapped using 0.25mm meshes in X and Y directions. The tool is divided into axial elements with a separation height of 0.1mm, and the cutter envelope points are generated for each 3° increment around the tool axis for each level. Simulations are carried out in MATLAB 2010a using a PC having Intel i5-450M processor (2.40GHz – DualCore) and 4 GB of RAM. Simulation times are given in Table 5.

Table 5: Simulation times for the process model

Operation	*Total step number*	*Sim. time*
I	617 steps	172.32s
II	614 steps	230.095s
III	232 steps	84.26s
IV	449 steps	252.616s

I

In Figure 18, the obtained machined surfaces are shown. Cutting forces were measured during the experiment using a rotary dynamometer (Kistler 9123). The results were not filtered. During the test no sign of chatter vibration was observed.

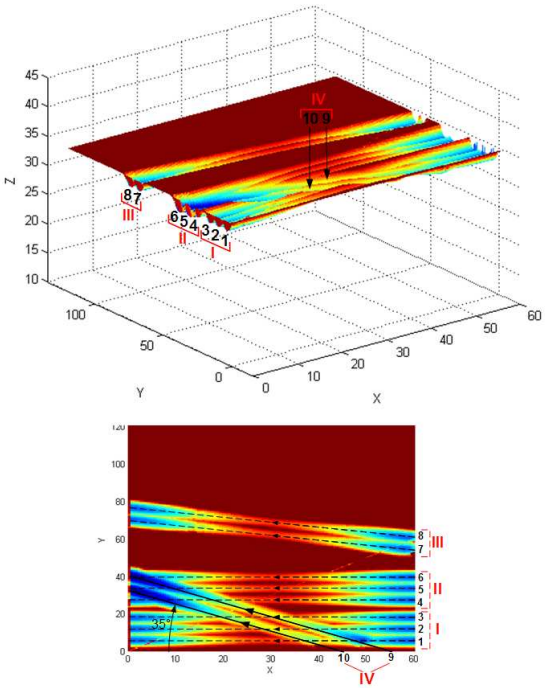

Figure 18: Simulated machined surface profiles from Z-mapping algorithm.

The process model utilizes the mechanistic force modeling approach and it is directly used in the Z-mapping algorithm as an auxiliary function. In Figure 19, the calculated and measured forces in *XY* workpiece coordinates are shown for each operation at every step. The simulated forces are the resultant of F_x and F_y. Only the maximum resultant forces from simulation and measurement results are compared. The results show that for 3 axis operations the process model can very closely predict the realistic measured forces (the first graph in Figure 19). However, in 5-axis machining cases, even though the cutting force trends are predicted satisfactorily, there is an offset with the measured maximum force values (the 2nd graph in Figure 19). For the final case where a previously machined surface is cut, even though the overall trend is captured, the prediction values are not very satisfactory. This difference can be attributed to the chosen simulation step numbers and the mesh size; increasing these values may yield better results. Moreover for the last case, the utilized Z-mapping algorithm was unable to capture the variation of the previously cut surface. The mapping and intersection method should be reconsidered and further improved.

5 CONCLUSION

In this study, a generalized process model is introduced encompassing all possible cutting tool geometries due to the numerical approach used in modeling. The strongest aspect of the proposed model is its robustness and flexibility to adapt compared to limited analytical models which are case specific. The verification tests carried out using various tool geometries yielded agreeable results. The process model is adapted to a Z-mapping process simulation algorithm and in-process continuous cutting forces for different tool geometries were calculated. Although verification tests for continuous process simulations produced some reasonable results, the simulation of 5-axis cycles needs to be improved.

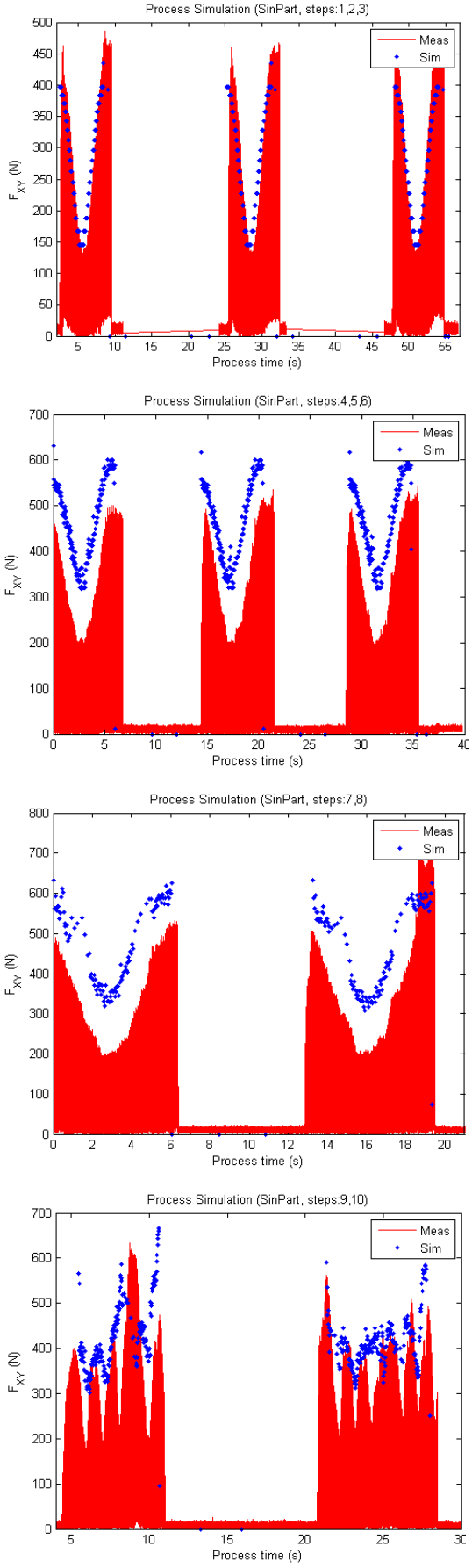

Figure 19: Simulated and measured process forces

References

[1] Martelotti, M. E., “An analysis of milling process”, Transactions of ASME, Vol. 122, pp.3-11, 1941.

[2] F. Koenigsberger, A.J.P. Sabberwal, “An investigation into the cutting force pulsations during milling operations, International Journal of Machine Tool Design and Research Vol. 1, pp 15–33, 1961.

[3] Kline, W. A., DeVor, R. E., Lindberg, J. R., “The prediction of cutting forces in the end milling with application to cornering cuts.”, International Journal of Machine Tool Design and Research, Vol. 22, pp.7-22, 1982.

[4] Altintas, Y., Spence, A., “End milling force algorithms for CAD systems”, CIRP Annals, Vol. 40, pp.7-22, 1991.

[5] Budak, E., Altintas, Y., Armarego, E.J.A., “Prediction of Milling Force Coefficients from Orthogonal Cutting Data”, Transactions of ASME, Vol. 118, pp. 216-224, 1996.

[6] Lee, P. and Altintas, Y., “A General Mechanics and Dynamics Model for Helical End Mills”, Annals of the CIRP, Vol.45, pp. 59-64, 1996.

[7] Lee, P., Altintas, Y., “Prediction of ball end milling forces from orthogonal cutting data”, International Journal of machine Tools and Manufacture, Vol.36, pp.1059-1072, 1996.

[8] Engin, S. and Altıntaş, Y.,“Mechanics and dynamics of general milling cutters. part I: helical end mills”, Int. Journal of Machine Tools & Manufacture. Vol.41, pp. 2213-2231, 2001.

[9] Tlusty, J., Ismail, F., Zaton, W., “Milling cutters with irregular pitch”, Technical report, McMaster Engineering Society, Canada

[10] Campomanes, M. L., “Kinematics and dynamics of milling with roughing endmills”, Metal Cutting and High Speed Machining, Kluwer Academic/Plenum Publishers, 2002.

[11] Altintas, Y., Budak, E., “Analytical prediction of stability lobes in milling”, Annals of the CIRP, Vol.44/1, pp.357-362, 1995.

[12] Merdol, S.D., Altintas, Y., “Mechanics and dynamics of serrated cylindrical and tapered end mills”, Journal of Manufacturing Science and Engineering, Vol.126, pp.217-236, 2004.

[13] Zhang, Z., Zheng, L. “A cutting force model for waved-edged end milling cutters”, International Journal of Advance Manufacturing Technology, Vol.21, pp.403-410, 2003.

[14] Lazoglu I., Liang, S. Y., “Modelling of ball-end milling forces with cutter inclination” Journal of Manufacturing Science and Enginnering, Vol.122., pp.3-11, 1996.

[15] Maeng, S. R., Baek, N., Shin, S.Y., Choi, B. K., “A Z-map update method for linear moving tools”, Computer-Aided Design, Vol. 35, pp.995-1009, 2003.

[16] Kim, G. M., Ko, S. L., “Improvement of cutting simulation using Octree method”, International Journal of Advance Manufacturing Technology, Vol.28, pp.1152-1160.

[17] Ozturk, E., Budak E., “Modeling of 5-axis milling processes”, Machine Science and Technology, Vol. 11/3, pp. 287-311, 2007.

[18] Lee, P., Altintas, Y., “Prediction of ball end milling forces from orthogonal cutting data”, International Journal of machine Tools and Manufacture, Vol.36, pp.1059-1072, 1996.

[19] Ferry, W. B., Altintas, Y., “Virtual five-axis flank milling of jet engine impellers – part I-II”, Journal of Manufacturing Science and Engineering, Vol.130, pp.011005, 2008.